ISSN (Print) 1226-1750
ISSN (Online) 2233-6656
**Journal of Magnetics** 22(2), 227-233 (2017) https://doi.org/10.4283/JMAG.2017.22.2.227

# Effects of Physical Factors on Computed Tomography Image Quality

**Min-Cheol Jeon[1], Man-Seok Han[2]*, Jae-Uk Jang[3], and Dong-Young Kim[4]**

*[1]Department of Radiology, Daejeon Health Institute of Technology, Daejeon 34504, Korea*
*[2]Department of Radiological Science, Kangwon National University, Samcheok 25949, Korea*
*[3]Department of Radiation Oncology, Chungnam National University Hospital, Daejeon 35015, Korea*
*and Department of Health Medical Science, Graduate School, Kangwon National University, Samcheok 25913, Korea*
*[4]Department of Biomedical Engineering, Chungnam National University, Daejeon 35015, Korea*

(Received 24 February 2017, Received in final form 11 April 2017, Accepted 11 April 2017)

**The purpose of this study was to evaluate the effects of X-ray photon energy, tissue density, and the kernel essential for image reconstruction on the image quality by measuring HU and noise. Images were obtained by scanning the RMI density phantom within the CT device, and HU and noise were measured as follows: images were obtained by varying the tube voltages, the tube currents and eight different kernels. The greater the voltage-dependent change in the HU value but the noise was decreased. At all densities, changes in the tube current did not exert any significant influence on the HU value, whereas the noise value gradually decreased as the tube current increased. At all densities, changes in the kernel did not exert any significant influence on the HU value. The noise value gradually increased in the lower kernel range, but rapidly increased in the higher kernel range. HU is influenced by voltage and density, and noise is influenced by voltage, current, kernel, and density. This affects contrast resolution and spatial resolution.**

**Keywords :** Hounsfield unit (HU), noise, kernel, tube voltage, tube current, density

## 1. Introduction

Computed Tomography (CT) scanning is an imaging procedure, wherein an object is imaged using the differences in X-ray attenuation when X-rays penetrate the object. Attenuation refers to the reduction in the intensity of X-rays due to absorption or scattering within matter [1]. Physical factors determining the degree of attenuation during a CT scan include the X-ray photon energy, tissue density, tissue atomic number, and number of electrons per unit mass of material (electrons/gram) [2]. These factors influence parameters of the CT image quality, such as Hounsfield units (HU) and noise. CT image quality plays an important role in diagnosing diseases because clear and precise imaging of the microstructures of the human body is essential for accurate diagnosis [3].

A CT scan makes use of the fact that the degree of X-ray attenuation varies in different tissues of the human body, which is expressed by HU or the CT number.

$$HU = 1000 \times \frac{\mu - \mu_w}{\mu_w} \tag{1}$$

The HU scale differs slightly from one CT scanner to another, but it is based on the attenuation coefficients of air (−1000 HU) and water (0 HU). The attenuation coefficients of a material and water are defined by $\mu$ and $\mu_w$, respectively, where $\mu$ depends on the atomic number

$$\mu = N_e\left(a\frac{Z_\tau^m}{E^k} + b\frac{Z_R^n}{E^l} + c(E)\right) \ (\mathrm{cm}^{-1}) \tag{2}$$

where $N_e$ is the electron density expressed in terms of the number of electrons per unit volume, $E$ is the photon energy, $Z_\tau$ and $Z_R$ are the effective atomic numbers for photoelectric absorption and Rayleigh scattering, respectively, and $a$, $b$, $m$, $n$, $k$, $l$ are calibration constants [5]. CT image quality is also influenced by the kernel used for converting raw data into image data [6]. This study was conducted to evaluate the effects of X-ray photon energy, tissue density, and the kernel essential for image reconstruction on the image quality by measuring HU and noise, the two major components of CT image quality.


*Corresponding author: Tel: +82-33-540-3383
Fax: +82-33-540-3389, e-mail: angio7896@naver.com

## 2. Materials and Methods

### 2.1. Equipment and materials

1. SOMATOM definition AS open (Siemens, Germany) CT
2. RMI CT density phantom (Gammex, USA)
3. PACS (Picture Archiving and Communication System) using m-view (INFINITT, Korea)

### 2.2. Experimental

All of the experiments in this study were conducted using a CT Electron Density Phantom (Gammex RMI, USA), a cylinder of 33 cm diameter, into which plugs of 12 different densities (0.28, 0.48, 0.943, 0.983, 1.016, 1.053, 1.106, 1.129, 1.146, 1.334, 1.599, and 1.822 g/cm$^3$) representing different human organs and structures (brain, liver, breast, etc.) can be placed. As X-ray equipment, the CT system SOMATOM Definition AS Open (Siemens, Germany) was used. Images were obtained by scanning the RMI density phantom within the CT device, and HU and noise were measured as follows:

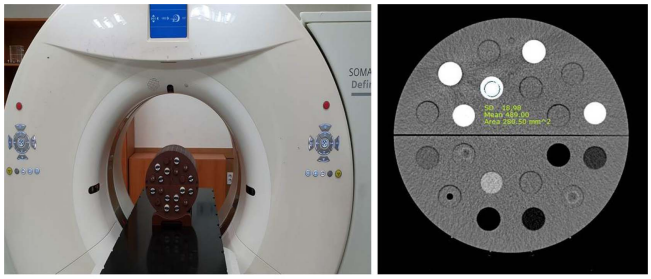

(a) (b)

**Fig. 1.** (Color online) The RMI CT density phantom was scaned with SOMATOM definition AS open CT (a). The HU and Noise of image scaned was measured with ROI of PACS (b).

1. Under a fixed tube current of 200 mAs and a slice thickness of 5 mm, images were obtained by varying the tube voltages (70, 80, 100, 120, and 140 kVp), This was followed by HU and noise measurements.
2. Under a fixed tube voltage of 100 kVp and a slice thickness of 5 mm, images were obtained by varying the tube currents (30, 60, 90, 120, 150, 180, 210, 240, 270, and 300 mAs). This was followed by HU and noise measurements.
3. Image reconstruction was performed on the images obtained under the conditions of slice thickness of 100 kVp, 210 mAs, and 5 mm, applying eight different kernels [B10 (very smooth), B20 (smooth), B30 (medium smooth), B40 (medium), B50 (medium sharp), B60 (sharp), B70 (very sharp), and B80 (ultrasharp)]. This was followed by HU and noise measurements.

The CT scan images were transferred to M-view, a PACS viewing software, and HU and noise values were measured after selecting regions of interest (ROIs).

## 3. Results

### 3.1. HU and noise according to tube voltage and density

After fixing the tube current at 200 mAs and choosing the kernel (B30), HU and noise values were measured by applying various tube voltages (70, 80, 100, 120, and 140 kVp) and densities (0.28, 0.48, 0.943, 0.983, 1.016, 1.053, 1.106, 1.129, 1.146, 1.334, 1.599, and 1.822 g/cm$^3$). Depending on the density, the HU values measured ranged −711.3-1877.3 HU at 70 kVp, −712.7-1645.3 HU at 80 kVp, −717.3-1355.0 HU at 100 kVp, −716.3-1188.3 HU at 120 kVp, and −719.7-1095.3 HU at 140 kVp. As the density increased from 0.28 g/cm$^3$ to 1.822 g/cm$^3$, the HU value increased. The lower the density, the smaller

**Table 1.** HU according to tube voltage and density.

| Phantom material | Density (g/cm$^3$) | HU | | | | |
|---|---|---|---|---|---|---|
| | | 70 kVp | 80 kVp | 100 kVp | 120 kVp | 140 kVp |
| LN-300 Lung | 0.28 | −711.3 | −712.7 | −717.3 | −716.3 | −719.7 |
| LN-450 Lung | 0.48 | −523.3 | −525.0 | −528.3 | −526.7 | −531.0 |
| Adipose | 0.943 | −115.7 | −106.3 | −94.7 | −88.3 | −83.7 |
| Breast | 0.983 | −60.3 | −54.7 | −49.3 | −46.3 | −44.3 |
| Solid water | 1.016 | 8.3 | 7.3 | 2.0 | 0.3 | 0.0 |
| Brain | 1.053 | −4.0 | 3.7 | 15.3 | 23.7 | 28.3 |
| Liver | 1.106 | 95.0 | 91.7 | 86.7 | 85.3 | 83.3 |
| Inner Bone | 1.129 | 328.0 | 277.3 | 218.3 | 186.0 | 165.7 |
| B-200 Bone | 1.146 | 357.0 | 307.7 | 244.3 | 211.0 | 191.3 |
| CB2-30 % | 1.334 | 659.0 | 581.3 | 489.0 | 436.3 | 406.7 |
| CB2-50 % | 1.599 | 1247.7 | 1090.3 | 902.7 | 796.0 | 735.0 |
| Cortical bone | 1.822 | 1877.3 | 1645.3 | 1355.0 | 1188.3 | 1095.3 |

**Table 2.** Noise according to tube voltage and density.

| Phantom material | Density ($g/cm^3$) | NOISE | | | | |
|---|---|---|---|---|---|---|
| | | 70 kVp | 80 kVp | 100 kVp | 120 kVp | 140 kVp |
| LN-300 Lung | 0.28 | 38.5 | 31.5 | 26.4 | 25.1 | 24.6 |
| LN-450 Lung | 0.48 | 36.5 | 26.2 | 18.0 | 14.8 | 14.0 |
| Adipose | 0.943 | 34.3 | 22.4 | 13.5 | 10.0 | 8.3 |
| Breast | 0.983 | 32.3 | 21.6 | 13.0 | 9.8 | 7.8 |
| Solid water | 1.016 | 35.4 | 24.6 | 13.8 | 10.9 | 8.2 |
| Brain | 1.053 | 40.1 | 26.9 | 15.5 | 10.9 | 9.2 |
| Liver | 1.106 | 40.2 | 25.9 | 15.1 | 11.6 | 9.8 |
| Inner Bone | 1.129 | 45.8 | 33.7 | 17.7 | 13.3 | 10.2 |
| B-200 Bone | 1.146 | 35.9 | 25.6 | 13.9 | 10.5 | 8.4 |
| CB2-30 % | 1.334 | 47.6 | 34.2 | 19.0 | 13.0 | 10.8 |
| CB2-50 % | 1.599 | 48.2 | 33.7 | 17.8 | 12.4 | 10.2 |
| Cortical bone | 1.822 | 55.7 | 35.0 | 20.6 | 15.0 | 12.3 |

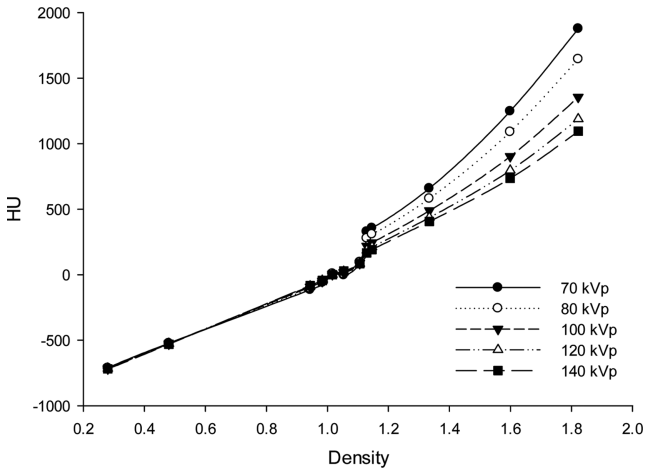


**Fig. 2.** Graph plotting the HU in the various tube voltages (70 kVp-140 kVp) and densities (0.28 $g/cm^3$-1.822 $g/cm^3$).

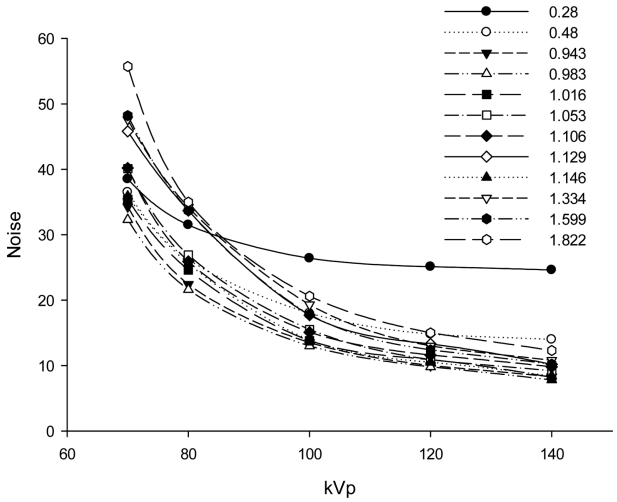


**Fig. 3.** Graph plotting the noise in the various tube voltages (70 kVp-140 kVp) and densities (0.28 $g/cm^3$-1.822 $g/cm^3$).

the voltage-dependent change in the HU value, and accordingly, the higher the density, the greater the voltage-dependent change in the HU value (Table 1).

Depending on the density, the measured noise ranged 32.3-55.7 at 70 kVp, 21.6-35.0 at 80 kVp, 13.0-26.4 at 100 kVp, 9.8-25.1 at 120 kVp, and 7.8-24.6 at 140 kVp. As the tube voltage increased from 70 kVp to 140 kVp, the noise decreased (Table 2).

### 3.2. HU and noise according to tube current and density

After fixing the tube voltage at 100 kVp and choosing the kernel (B30), HU and noise values were measured, applying various tube currents (30, 60, 90, 120, 150, 180, 210, 240, 270, and 300 mAs) and densities (0.28, 0.48, 0.943, 0.983, 1.016, 1.053, 1.106, 1.129, 1.146, 1.334, 1.599, and 1.822 $g/cm^3$). The measured values of HU and noise ranged −718.3-1353.3 HU and 33.7-50.4 at 30 mAs, −718.3-1361.7 HU and 22.7-37.8 at 60 mAs, −718.3-1358.7 HU, 19.4-30.2 at 90 mAs, −717.0-1354.3 HU and 17.5-28.1 at 120 mAs, −716.7-1353.7 HU and 15.3-28.0 at 150 mAs, −717.0-1354.7 HU and 13.8-25.9 at 180 mAs, −717.7-1354.3 HU and 12.0-26.2 at 210 mAs, −716.3-1354.7 HU and 12.0-26.6 at 240 mAs, −716.3-1353.0 HU and 10.9-25.5 at 270 mAs, and −716.0-1355.7 HU and 10.6-26.5 at 300 mAs. At all densities, changes in the tube current did not exert any significant influence on the HU value, whereas the noise value gradually decreased as the tube current increased from 30 mAs to 300 mAs (Tables 3 and 4).

### 3.3. HU and noise according to kernel

CT images were obtained with X-ray photon energy

**Table 3.** HU according to tube current and density.

| Phantom material | Density (g/cm$^3$) | HU | | | | | | | | | |
|---|---|---|---|---|---|---|---|---|---|---|---|
| | | 30 mAs | 60 mAs | 90 mAs | 120 mAs | 150 mAs | 180 mAs | 210 mAs | 240 mAs | 270 mAs | 300 mAs |
| LN-300 Lung | 0.28 | –718.3 | –718.3 | –718.3 | –717.0 | –716.7 | –717.0 | –717.7 | –716.3 | –716.3 | –716.0 |
| LN-450 Lung | 0.48 | –531.3 | –528.0 | –529.0 | –528.3 | –527.7 | –528.3 | –527.7 | –527.0 | –528.0 | –527.0 |
| Adipose | 0.943 | –94.7 | –94.7 | –95.0 | –95.3 | –95.3 | –94.7 | –95.3 | –95.0 | –96.3 | –95.3 |
| Breast | 0.983 | –49.0 | –49.7 | –50.3 | –49.7 | –49.0 | –50.0 | –50.7 | –50.0 | –50.3 | –50.0 |
| Solid water | 1.016 | 4.7 | 3.0 | 2.3 | 0.7 | 1.7 | 2.0 | 2.0 | 1.3 | 1.7 | 2.0 |
| Brain | 1.053 | 20.3 | 15.7 | 15.7 | 16.0 | 15.7 | 16.3 | 15.0 | 16.3 | 15.7 | 15.7 |
| Liver | 1.106 | 91.0 | 86.3 | 85.3 | 85.3 | 87.0 | 86.3 | 87.0 | 86.3 | 86.0 | 86.3 |
| Inner Bone | 1.129 | 223.7 | 221.3 | 219.7 | 219.0 | 219.0 | 218.7 | 218.3 | 218.3 | 218.0 | 218.3 |
| B-200 Bone | 1.146 | 249.3 | 248.0 | 245.3 | 245.0 | 244.0 | 245.0 | 245.3 | 245.3 | 244.7 | 245.7 |
| CB2-30 % | 1.334 | 491.3 | 489.7 | 490.7 | 489.7 | 489.7 | 490.3 | 488.7 | 488.3 | 488.7 | 488.7 |
| CB2-50 % | 1.599 | 906.0 | 906.0 | 904.7 | 903.7 | 901.7 | 902.0 | 901.3 | 907.7 | 902.7 | 902.0 |
| Cortical bone | 1.822 | 1353.3 | 1361.7 | 1358.7 | 1354.3 | 1353.7 | 1354.7 | 1354.3 | 1354.7 | 1353.0 | 1355.7 |

**Table 4.** Noise according to tube current and density.

| Phantom material | Density (g/cm$^3$) | NOISE | | | | | | | | | |
|---|---|---|---|---|---|---|---|---|---|---|---|
| | | 30 mAs | 60 mAs | 90 mAs | 120 mAs | 150 mAs | 180 mAs | 210 mAs | 240 mAs | 270 mAs | 300 mAs |
| LN-300 Lung | 0.28 | 38.8 | 33.1 | 28.6 | 28.1 | 28.0 | 25.9 | 26.2 | 26.6 | 25.5 | 26.5 |
| LN-450 Lung | 0.48 | 37.6 | 29.4 | 23.7 | 20.3 | 15.3 | 19.0 | 18.6 | 18.0 | 15.0 | 16.7 |
| Adipose | 0.943 | 35.6 | 24.1 | 20.6 | 17.5 | 15.3 | 14.1 | 13.4 | 12.5 | 11.7 | 12.0 |
| Breast | 0.983 | 33.7 | 22.7 | 19.4 | 18.2 | 15.6 | 13.8 | 12.0 | 12..1 | 10.9 | 10.6 |
| Solid water | 1.016 | 36.6 | 26.9 | 22.6 | 17.6 | 16.0 | 15.4 | 12.4 | 12.1 | 11.5 | 11.1 |
| Brain | 1.053 | 39.0 | 28.4 | 24.2 | 21.0 | 17.9 | 16.4 | 15.0 | 15.1 | 13.5 | 12.4 |
| Liver | 1.106 | 40.2 | 27.6 | 22.3 | 21.4 | 17.9 | 16.3 | 15.4 | 14.2 | 12.9 | 13.6 |
| Inner Bone | 1.129 | 44.9 | 33.4 | 27.5 | 23.0 | 20.5 | 18.7 | 17.4 | 17.4 | 15.5 | 15.0 |
| B-200 Bone | 1.146 | 36.7 | 25.3 | 21.2 | 20.3 | 16.7 | 15.1 | 13.5 | 12.0 | 12.4 | 11.7 |
| CB2-30 % | 1.334 | 44.2 | 35.4 | 27.9 | 25.4 | 22.5 | 20.1 | 19.3 | 17.2 | 16.1 | 15.5 |
| CB2-50 % | 1.599 | 44.0 | 33.9 | 26.2 | 21.7 | 20.0 | 18.2 | 16.8 | 16.1 | 14.3 | 14.0 |
| Cortical bone | 1.822 | 50.4 | 37.8 | 30.2 | 26.6 | 22.0 | 20.1 | 19.8 | 18.4 | 17.1 | 15.8 |

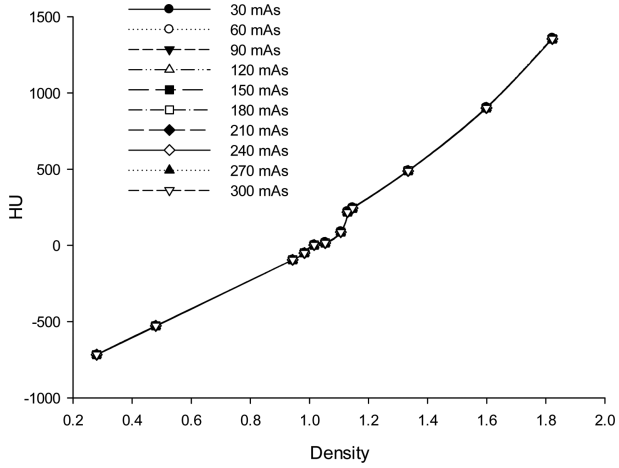


**Fig. 4.** Graph plotting the HU in the various tube currents (30 mAs-300 mAs) and densities (0.28 g/cm$^3$-1.822 g/cm$^3$).

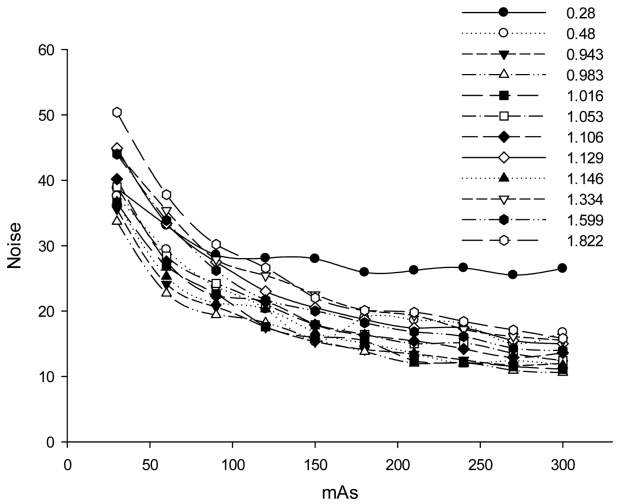


**Fig. 5.** Graph plotting the noise in the various tube currents (30 mAs-300 mAs) and densities (0.28 g/cm$^3$-1.822 g/cm$^3$).

**Table 5.** HU according to kernel.

| Phantom material | Density (g/cm$^3$) | HU | | | | | | | |
|---|---|---|---|---|---|---|---|---|---|
| | | B10 | B20 | B30 | B40 | B50 | B60 | B70 | B80 |
| LN-300 Lung | 0.28 | −712.3 | −710.3 | −717.7 | −709.0 | −707.3 | −707.0 | −707.0 | −710.0 |
| LN-450 Lung | 0.48 | −530.7 | −525.7 | −527.7 | −524.0 | −522.3 | −522.7 | −523.3 | −524.3 |
| Adipose | 0.943 | −95.0 | −95.0 | −95.3 | −94.7 | −94.0 | −95.0 | −94.3 | −94.3 |
| Breast | 0.983 | −50.3 | −49.0 | −50.7 | −49.0 | −49.0 | −49.7 | −49.3 | −49.7 |
| Solid water | 1.016 | 2.3 | 2.3 | 2.0 | 2.3 | 2.0 | 1.3 | 1.3 | 2.0 |
| Brain | 1.053 | 15.7 | 15.7 | 15.0 | 15.7 | 15.3 | 17.0 | 17.0 | 16.0 |
| Liver | 1.106 | 86.3 | 86.3 | 87.0 | 86.0 | 86.0 | 86.0 | 85.7 | 85.0 |
| Inner Bone | 1.129 | 218.7 | 215.7 | 218.3 | 216.3 | 214.3 | 213.3 | 213.3 | 214.3 |
| B-200 Bone | 1.146 | 244.3 | 243.3 | 245.3 | 243.0 | 243.0 | 243.7 | 243.7 | 243.7 |
| CB2-30 % | 1.334 | 486.3 | 484.7 | 488.3 | 483.7 | 483.0 | 492.3 | 492.7 | 496.3 |
| CB2-50 % | 1.599 | 906.0 | 895.3 | 901.3 | 893.3 | 891.3 | 893.0 | 893.0 | 894.7 |
| Cortical bone | 1.822 | 1362.3 | 1340.7 | 1354.3 | 1337.0 | 1335.0 | 1336.3 | 1336.3 | 1338.3 |

**Table 6.** Noise according to kernel.

| Phantom material | Density (g/cm$^3$) | NOISE | | | | | | | |
|---|---|---|---|---|---|---|---|---|---|
| | | B10 | B20 | B30 | B40 | B50 | B60 | B70 | B80 |
| LN-300 Lung | 0.28 | 16.5 | 18.2 | 26.2 | 21.9 | 41.2 | 76.5 | 85.9 | 89.6 |
| LN-450 Lung | 0.48 | 14.1 | 13.1 | 18.6 | 19.1 | 41.7 | 81.8 | 91.8 | 95.0 |
| Adipose | 0.943 | 8.8 | 11.1 | 13.4 | 16.2 | 38.2 | 75.8 | 85.1 | 87.3 |
| Breast | 0.983 | 8.5 | 10.4 | 12.0 | 15.1 | 36.2 | 74.0 | 82.7 | 83.6 |
| Solid water | 1.016 | 9.3 | 10.7 | 12.4 | 15.9 | 38.4 | 76.7 | 86.2 | 88.4 |
| Brain | 1.053 | 8.1 | 10.6 | 15.0 | 16.7 | 40.5 | 84.8 | 94.9 | 95.2 |
| Liver | 1.106 | 9.4 | 12.1 | 15.4 | 18.1 | 40.3 | 80.1 | 90.1 | 92.3 |
| Inner Bone | 1.129 | 11.3 | 13.9 | 17.4 | 20.2 | 44.6 | 89.7 | 100.4 | 102.3 |
| B-200 Bone | 1.146 | 9.6 | 11.9 | 13.5 | 17.1 | 39.8 | 79.7 | 89.8 | 91.1 |
| CB2-30 % | 1.334 | 10.7 | 13.8 | 19.3 | 20.7 | 47.4 | 94.6 | 108.1 | 109.2 |
| CB2-50 % | 1.599 | 12.0 | 13.7 | 16.8 | 19.9 | 47.2 | 94.5 | 105.2 | 107.8 |
| Cortical bone | 1.822 | 14.4 | 15.3 | 19.8 | 21.6 | 51.1 | 100.8 | 113.3 | 116.1 |

fixed at 100 kVp and 210 mAs, and HU and noise were measured, applying eight different kernels (B10-B80). HU and noise ranged −712.3-1362.3 HU and 8.1-16.5 at B10, −710.3-1340.7 HU and 10.4-18.2 at B20, −717.7-1354.3 HU and 12.0-26.2 at B30, −709.0-1337.0 HU and 15.1-21.9 at B40, −707.3-1335.0 HU and 36.2-51.1 at

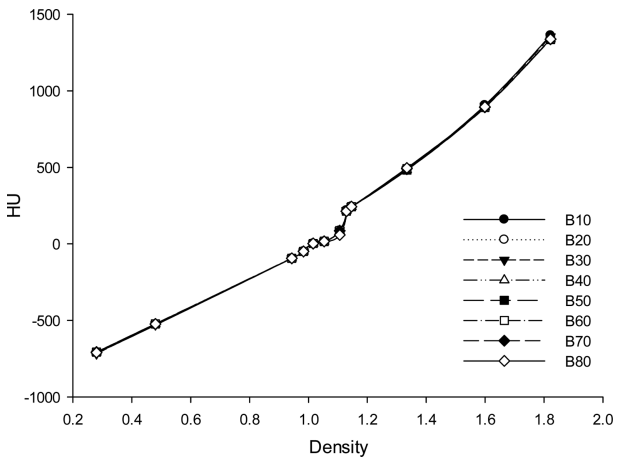


**Fig. 6.** Graphs plotting the HU values in the various kernels (B10-B80) and densities (0.28 g/cm$^3$-1.822 g/cm$^3$).

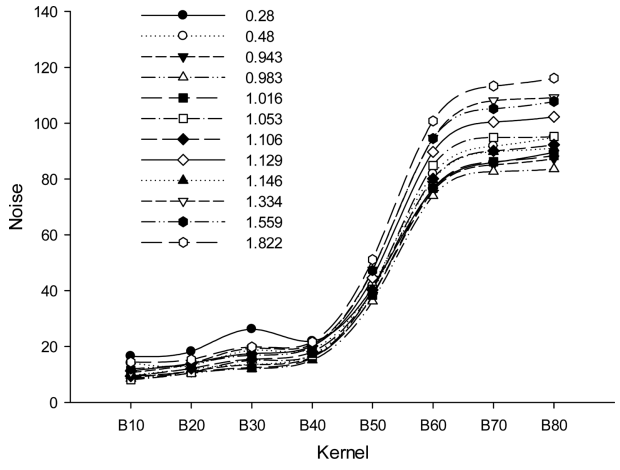


**Fig. 7.** Graphs plotting the noise values in the various kernels (B10-B80) and densities (0.28 g/cm$^3$-1.822 g/cm$^3$).

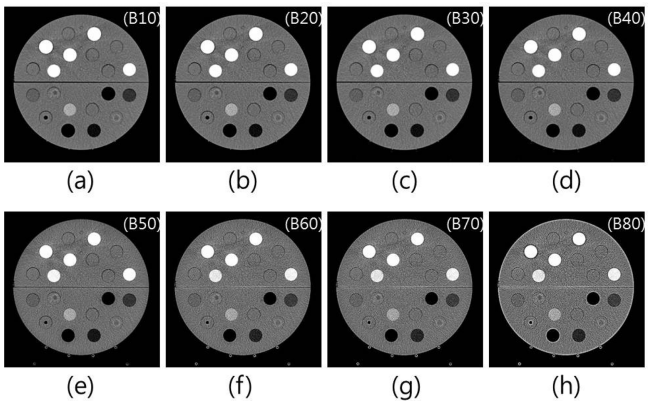


**Fig. 8.** The image of the phantom reconstructed with kernels. Eight images were reconstructed with various kernels as follows: (a) very smooth, (b) smooth, (c) medium smooth, (d) medium, (e) medium sharp, (f) sharp, (g) very sharp, (h) ultra sharp.

B50, −707.0-1336.3 HU and 74.0-100.8 at B60, −707.0-1336.3 HU and 82.7-113.3 at B70, and −710.0-1338.3 HU and 83.6-116.1 at B80. At all densities, changes in the kernel did not exert any significant influence on the HU value. The noise value gradually increased in the lower kernel range (B10-B40), but rapidly increased in the higher kernel range (B50-B80) (Tables 5 and 6).

## 4. Discussion

CT scan plays an important role in diagnostic and therapeutic decision-making because it has high diagnostic accuracy [7-9]. Since CT images should depict microstructures with great precision, it is of paramount importance to evaluate the effects of factors determinant of image quality [10]. This study investigated the effects of X-ray photon energy, tissue electron density, and kernel on the image quality by varying their values in the ranges of 70-140 kVp, 0.28-1.822 g/cm$^3$ and B10-B80, respectively.

Attenuation occurs as a result of absorption and scattering. As is the case with general radiography, attenuation by the photoelectric effect or scattering by the Compton effect is involved in CT. The total attenuation can thus be defined by the equation below.

$$I = I_0 e^{-(\mu_p + \mu_c)x}$$

Here, $I$ is the intensity after the permeation, $I_0$ is the original intensity, $e$ is the base of natural logarithm, $\mu_p$ is the linear attenuation coefficient resulting from the photoelectric effect, and $\mu_c$ is the linear attenuation coefficient resulting from the Compton effect. In a CT device, such a distribution of the attenuation values is expressed by the CT number [6].

According to the experimental results of this study, as the tube voltage increases from 70 kVp to 140 kVp, X-ray energy attenuation is not large at low densities, resulting in low HU values; the HU value increases at higher densities, owing to increased X-ray energy attenuation. A higher HU value yielded at 70 kVp because of the smaller X-ray energy than at 140 kVp results in higher attenuation. Moreover, given that X-ray radiation is polychromatic with diverse energies, the HU value increases exponentially with increasing density, as depicted in Fig. 2, unlike monochromatic radiation with a homogeneous beam. The difference in HU contributes to increasing the image contrast. Table 2 shows that noise decreases as the tube voltage increases. This may be interpreted as the result of decreased quantum noise due to the increased number of photons reaching the sensor owing to the effect of increased X-ray permeability with increasing X-ray energy.

While the increase in tube current from 30 mAs to 300 mAs does not affect the HU value significantly at the same density, noise is reduced. This is due to the fact that a higher tube current does not boost the beam quality, but increases the beam quantity, which results in quantum noise reduction, which increases the image contrast resolution.

CT scan data are converted into image data using kernel. According to the experimental results of this study, an increase in kernel from B10 to B80 does not change the HU value significantly, but increases noise. This is ascribable to the noise generation through the filter applied in the reconstruction kernel. Owing to the fact that HU and noise change little in the lower kernel range, kernels B10-B40 are applied to the regions with low attenuation coefficients, such as the abdomen, and kernels B60 or higher are well-suited for bones with clear boundaries, organs with pneumatic anatomy, and regions with high attenuation coefficients. As a mid-range kernel, B50 has characteristics that lie between the kernels with high contrast resolution suitable for regions with low attenuation coefficients such as abdomen and kernels with high spatial resolution suitable for bone and air, and should be used for soft tissue and regions of the spine for bone observation.

As a limitation of this study, it should be pointed out that only one phantom type and one slice thickness were used. Therefore, noise measurements according to object and slice thicknesses could not be made, although they affect noise. A follow-up study can be performed varying the object and slice thicknesses as well.

## 5. Conclusion

This study found that HU is influenced by voltage and density, and noise is influenced by voltage, current, kernel, and density. This affects contrast resolution and spatial resolution. Therefore, in order to improve resolution, X-ray photon energies and kernels appropriate for each scan region and purpose should be selected. As a result, the improvement of resolution enhance accuracy of diagnosis by distinguishing micro lesions.

## References

[1] H. C. Jang, Y. S. Kim, and H. J. Kim, J. The Korea Academia-Industrial Cooperation Soc. **15**, 1584 (2014).
[2] S. M. Ha, S. H. Jung, H. J. Chang, E. A. Park, and H. J. Shim, J. Progress in Med. Phys. **26**, 28 (2015).
[3] E. J. Balthazar, A. J. Megibow, D. Hulnick, D. P. Naidich, Am. J. Roentgenol. **150**, 301 (1988).
[4] H. M. Lee, B. G. Yoo, and D. C. Keon, J. Radiological Science and Technol. **31**, 71 (2008).
[5] K. Ogden, W. Huda, E. M. Scalzetti, and M. L. Roskopf, Health Phys. **86**, 397 (2004).
[6] G. N. Hounsfield, Br. J. Radiol. **68**, H166 (1995).
[7] S. W. Lee, H. J. Kim, T. H. Kim, S. J. Jo, and C. L. Lee, J. Med. Phys. **20**, 145 (2009).
[8] S. K. Kang, B. C. Cho, H. C. Park, and H. S. Bae, J. Med. Phys. **15**, 23 (2004).
[9] J. U. Jang, M. S. Han, M. J. Kim, and H. S. Kang, J. Magn. **26**, 173 (2016).
[10] Y. Watanabe, Phys. Med. Biol. **44**, 2201 (1999).
[11] Chung-ku Publishing, Textbook of Computed Tomography, Korea (2009) pp. 47-75.
[12] E. Gallagher, T. Lukens, S. Colussiello, D. Morgan, S. Cantrill, and M. Campbell, Ann. Emerg. Med. **36**, 406 (2000).
[13] B. Siewert, V. Raptopoulos, M. F. Mueller, M. P. Rosen, and M. Steer, Am. J. Roentgenol. **168**, 173 (1997).
[14] R. K. Zeman, S. H. Fox, P. M. Silverman, W. J. Davros, L. M. Carter, and D. Griego, Am. J. Roentgenol. **160**, 719 (1993).
[15] M. C. Jeon, M. S. Han, J. U. Jang, Y. K. Kim, S. Y. Seo, and G. J. Kim, Cluster Comput. **19**, 931 (2016).